catalysts

MDPI

Article

Coke Formation and Regeneration during Fe-ZSM-5-Catalyzed Methane Dehydro-Aromatization

Sanjana Karpe and Götz Veser *

Department of Chemical and Petroleum Engineering, University of Pittsburgh, Pittsburgh, PA 15260, USA; svk10@pitt.edu
* Correspondence: gveser@pitt.edu

Abstract: Coke formation poses a significant obstacle in the direct conversion of methane into valuable chemicals such as ethylene, benzene, and hydrogen via methane dehydro-aromatization (MDA). At the elevated temperatures necessary for this reaction, coke is the thermodynamically favored product, causing rapid catalyst deactivation and hence necessitating frequent catalyst regeneration. Successful industrial implementation of MDA requires the advancement of catalyst regeneration processes and a comprehensive understanding of coke formation to enhance catalyst performance. Here, we examined the types of coke generated during MDA over a Fe-ZSM-5 catalyst and their impact on deactivation. By combining reactivity studies using catalysts with carefully controlled coke populations with the characterization of the catalyst via XRD, H_2-TPR, and pyridine FTIR, we find that soft coke is formed at the Brønsted acid sites, resulting in loss of selectivity, while hard coke is formed at the metal sites causing a loss of activity. While soft coke can be removed at low regeneration temperatures, the removal of hard coke requires harsh conditions which compromise catalyst stability. An investigation into the use of CO_2 as an alternative, mild oxidant for catalyst regeneration, however, shows that the mild oxidation strength of CO_2 requires even higher regeneration temperatures and hence irreversible loss of Brønsted acid sites.

Keywords: methane dehydro-aromatization; Fe-ZSM-5; soft coke; hard coke; regeneration

Citation: Karpe, S.; Veser, G. Coke Formation and Regeneration during Fe-ZSM-5-Catalyzed Methane Dehydro-Aromatization. *Catalysts* **2024**, *14*, 292. https://doi.org/10.3390/catal14050292

Academic Editor: Avelina García-García

Received: 6 April 2024
Revised: 25 April 2024
Accepted: 25 April 2024
Published: 26 April 2024

1. Introduction

Converting methane directly into valuable chemicals such as ethylene, benzene, and hydrogen via methane dehydro-aromatization (MDA) is an attractive pathway for methane utilization. The reaction is typically catalyzed by metal-embedded zeolites in which methane is first activated on a metal site to form CH_x species which desorb and dimerize to C_2 species in the gas phase. Further oligomerization of these C_2 species to aromatics then takes place on the Brønsted acid sites (BAS) of the zeolite, with the zeolite further providing shape selectivity towards the desired product benzene. A significant challenge in MDA is the formation of coke at the high temperature thermodynamically required to attain significant methane conversion (typically > 700 °C). At these temperatures, coke is generated both by methane deep dehydrogenation at the metal site and by the polymerization of intermediate species to heavy aromatics at the zeolite's Brønsted acid sites, resulting in rapid catalyst deactivation.

Coking-induced catalyst deactivation is a common challenge during hydrocarbon processing when using zeolites. Therefore, significant research efforts have focused on exploring various regeneration methods for zeolite catalysts. For example, the effect of regeneration temperature on the regeneration of spent ZSM-5 catalysts in the catalytic fast pyrolysis of biomass was identified and analysis of the regenerated samples revealed that oxidative treatment increased catalyst porosity by converting Brønsted acid sites to Lewis acid sites; the regeneration process thus influenced both catalyst structure and acidity, and hence catalyst activity [1]. Additionally, coke formation on ZSM-5-based, ZrO_2-promoted

extrudates was examined during catalytic fast pyrolysis of biomass, and optimal oxidative regeneration temperatures were determined to effectively remove coke without adversely affecting the catalyst's structure and acid sites [2]. Alternative regeneration methods, such as the use of non-thermal plasma, have also been explored to regenerate coked zeolite catalysts [3,4].

Fundamental studies on the mechanisms of coke formation and deactivation in hydrocarbon processing catalysts have yielded the first insights into the nature and impact of the different forms of coke formed [5]. In processes susceptible to coke deposition, such as reforming, the properties of coke are typically characterized via four primary characteristics: oxidation temperature, location on the catalyst surface, morphology, and chemical nature [6]. Various deactivation mechanisms have been discussed, including strong chemisorption leading to monolayer carbide formation, physisorption hindering active metal site access, total covering of active sites causing inaccessibility to reactants, plugging of micropores and/or mesopores, and changes or disintegration of catalyst structure and reactor plugging during advanced coke growth stages. A recent review by Weckhuysen and coworkers provides a lucid overview of various mechanisms of coke formation, including metal-induced soft coke formation on bifunctional catalysts, among others [5]. It is crucial to note that catalyst properties play a pivotal role in coke formation and deactivation. Notably, during the oligomerization of 1-butene using H-ZSM-5 embedded in a mesoporous matrix of γ-Al_2O_3 and α-Al_2O_3, two distinct types of coke emerged: soft coke, comprised of oligomers, and hard coke, consisting of more developed carbonaceous species. The influence of reaction conditions on the formation of these types of coke and strategies for the efficient removal of both types of coke was furthermore explored [7]. Examination of coke formation on Ni/ZSM-5 during ethylene oligomerization, employing state-of-the-art techniques such as high-resolution mass spectrometry allowed Hita et al. to unravel the temporal evolution of coke species at a molecular level, providing invaluable insights directly linked to catalytic performance [8]. These fundamental studies play a vital role in advancing our understanding of coke formation and growth mechanisms. The knowledge developed can contribute to the development of more efficient catalyst designs and improve the effectiveness of regeneration processes.

In the context of methane dehydro-aromatization (MDA), most attention has focused on studying coking and deactivation mechanisms in Mo-embedded zeolite catalysts. Donut-shaped Mo/HZSM-5 catalysts, designed with a lower diffusion pathway, were shown to improve catalyst stability by shifting the location of coke from micropores to mesopores [9]. Kosinov et al. investigated the carbonaceous species formed during Mo/zeolite-catalyzed MDA and related the distinction between hard and soft coke to their location within pores and on the external surface, respectively [10]. Furthermore, soft coke with a lower oxidation temperature was reported to be in close proximity to the Mo species, which helped catalyze the oxidation reaction during regeneration [11].

Traditionally, the regeneration of the MDA catalyst involves the combustion of coke using strong oxidants like air or oxygen. However, the high local heat generated from this strongly exothermic reaction can lead to severe sintering and irreversible damage to the catalyst. CO_2 as a potential alternative mild oxidant for regeneration could counter this issue. CO_2 oxidizes coke via the Boudouard reaction ($C + CO_2 \rightarrow CO$), an endothermic process, thereby lowering the local high temperature and potentially alleviating catalyst deactivation. CO_2 regeneration has been studied previously for coked catalysts in the FCC process. Santos et al. investigated the regeneration of coked FCC catalysts in a CO_2/He atmosphere and found that the type of coke has a notable effect on the gasification rate with aliphatic and poly-substituted aromatic species particularly prone to reacting with CO_2 [12]. Similarly, CO_2 gasification has been employed to regenerate Ni-Al_2O_3 catalysts for bio-oil reforming where it was found to be more beneficial than steam regeneration, which required large amounts of water, while O_2 regeneration led to catalyst sintering [13]. However, incomplete activity was restored through CO_2 regeneration. In contrast, complete

recovery of coked Ni catalysts via CO_2 regeneration has been reported for dry reforming of methane (DRM) [14].

Additionally, the regeneration of coked catalysts results in a substantial release of CO_2, a greenhouse gas and major contributor to climate change. For example, regenerating spent catalysts in FCC units through air combustion accounts for approximately 40–45% of CO_2 emissions from refineries [8,15]. Regeneration using CO_2 as an oxidant could contribute to the mitigation of these emissions while generating CO via the Boudouard reaction, which could then be further utilized to produce valuable chemicals.

While numerous approaches to the mitigation of coke formation and deactivation have been explored, coking continues to pose a major challenge, and further improvements in our understanding of the mechanisms of coke formation and removal in MDA are needed. Moreover, most in-depth studies to date have focused on Mo-ZSM-5 catalysts [10,16–18]. Coke formation on other metal-exchanged zeolites, including Fe-ZSM-5, has not been thoroughly explored. In the present work, we aimed to address this gap by investigating coke formation during MDA in Fe-ZSM-5 catalysts. We investigated the different types of coke produced during MDA in a Fe-ZSM-5 catalyst, their location on the different active sites, and their effects on MDA reactivity performance, and explored the use of CO_2 as an alternative oxidant for regeneration. With these studies, we aimed to shed light on the coking and regeneration of Fe-ZSM5 catalysts for methane dehydro-aromatization and thus enhance our understanding of MDA, inform the development of more efficient regeneration processes, and help move these reactions further towards commercial realization.

2. Results and Discussion

2.1. Catalyst Synthesis and Characterization

H-(Fe)-ZSM-5 was synthesized by a hydrothermal synthesis route in which Fe was incorporated into the zeolite framework [19,20] (see scheme in Figure 1; detailed synthesis procedure is provided in the Experimental Section). The catalyst was then characterized via XRD, SEM/EDX, and UV-Vis analysis to determine its crystallinity, morphology, composition, and Fe species distribution, respectively.

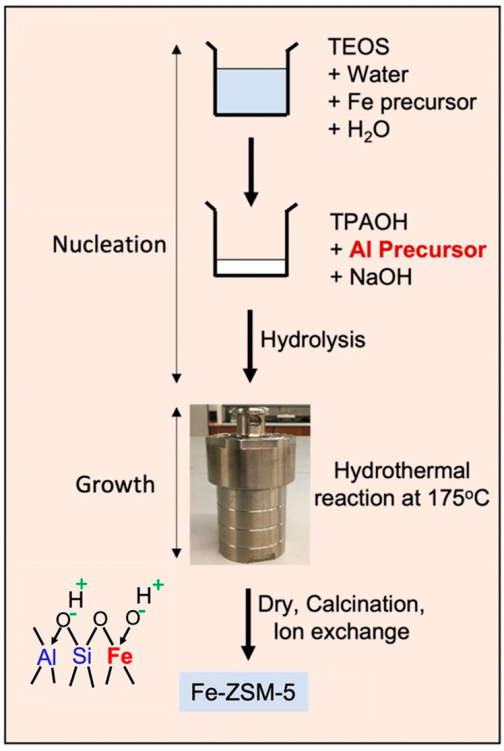

Figure 1. Synthesis procedure for isomorphously substituted Fe-ZSM-5 catalyst.

XRD analysis of the Fe-ZSM-5 sample (see Figure 2a) shows characteristic diffraction peaks corresponding to the zeolite MFI structure, with major peaks at 7.9° and 8.9°, as well as a characteristic triplet at 23.5°, confirming the formation of a well-crystalline Fe-ZSM-5 phase. Crystallite size was determined from Scherrer's equation, using the characteristic peak at 7.9°, to be 57.4 nm.

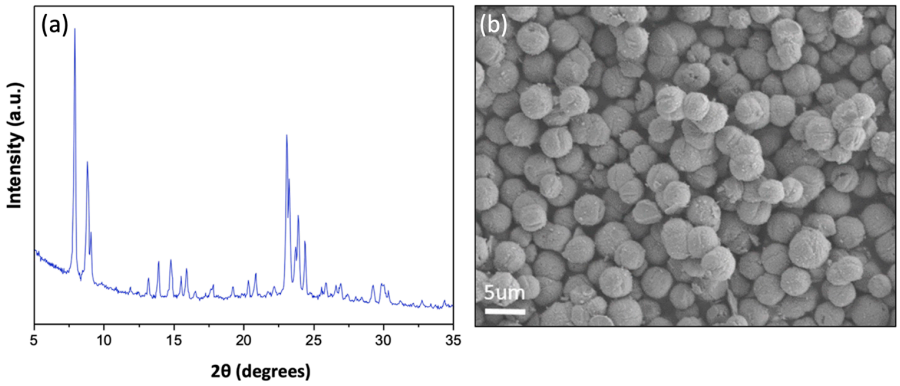

Figure 2. (**a**) X-ray diffraction analysis of Fe-ZSM-5 showing MFI peaks. (**b**) Scanning electron microscope image of synthesized Fe-ZSM-5. Synthesis conditions for pure Fe-ZSM-5 (molar ratios): Si/Fe = 46.1, Si/Al = 40, TPAOH/TEOS = 0.1, NaOH/TEOS = 0.2, H_2O/TEOS = 40.45, temperature = 175 °C.

SEM images (Figure 2b) show the formation of uniform Fe-ZSM-5 particles with an average size of ~4 μm. Table 1 shows the EDX compositional analysis of the isomorphous Fe-ZSM-5 catalyst with a target Fe loading of 2 wt.% and a target Si/Al ratio of 40. The analysis yielded an average Fe weight loading of 2.12 wt.% and a Si/Al ratio of 36.2 for the Fe-ZSM-5 sample, in good alignment with the target values.

Table 1. EDX compositional analysis of the isomorphous Fe-ZSM-5 catalyst.

Element	Wt.%	Mol.%
O	49.4 ± 1.76	63.6 ± 1.6
Al	1.25 ± 0.05	0.96 ± 0.038
Si	47.2 ± 1.56	34.6 ± 1.51
Fe	2.12 ± 0.21	0.78 ± 0.08
Total	100	
Si/Al		36.2

Nitrogen sorption analysis (BET analysis) was conducted on the as-synthesized Fe-ZSM-5 sample to determine its specific surface area (see Figure S1), which was found to be 412.12 m^2/g.

UV-Vis spectroscopy was used to analyze the distribution of Fe species in the isomorphous Fe-ZSM-5 sample (Figure 3). The absorption bands at 209 and 239 nm correspond to isolated Fe^{3+} in tetrahedral coordination, while the band at 282 nm indicates isolated Fe^{3+} in octahedral coordination [21–23]. Iron (Fe) incorporated into the zeolite framework is tetrahedrally coordinated, replacing Si atoms, while Fe at the exchange sites can exhibit either tetrahedral or octahedral coordination [20]. The absorption peaks at 300–450 nm are associated with small oligonuclear clusters (Fe_xO_y), and the bands above 450 nm are indicative of larger Fe_2O_3 particles [20–23]. These UV-Vis peaks reflect the varying cluster geometries and sizes of aggregated Fe species. According to the Kubelka–Munk theory, absorption is directly proportional to concentration, which facilitates the quantification of Fe species distribution from the UV-Vis spectra. UV-Vis analysis verifies that the majority

of Fe species are dispersed either within the framework or at the metal exchange site in Fe-ZSM-5 catalysts prepared via the isomorphous substitution method, which is recognized for producing isolated Fe species. However, a small fraction of Fe_2O_3 oligonuclear clusters was also detected.

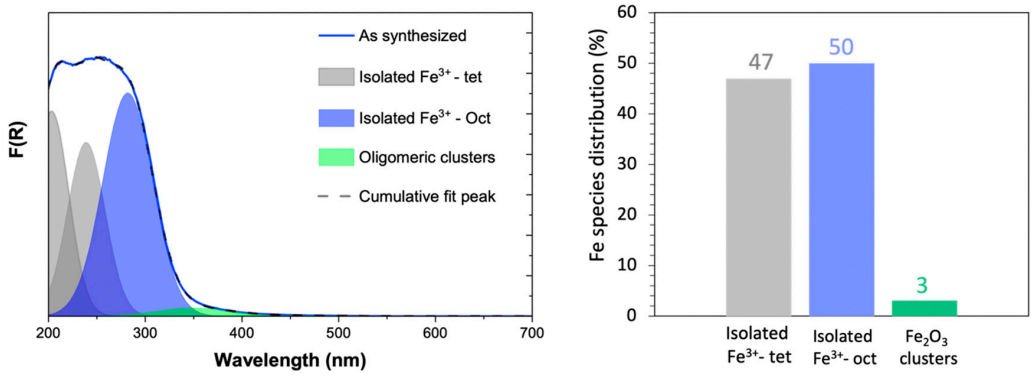

Figure 3. UV-Vis analysis on isomorphous as-synthesized Fe-ZSM-5 catalyst to determine Fe species distribution.

2.2. Effect of Varying Types of Coke on MDA Reactivity

To determine the varying types of coke formed during MDA, a temperature-programmed oxidation (TPO) was conducted on a coked and deactivated catalyst sample after 14 h operation of MDA at 700 °C in a 50:50 CH_4:Ar environment at WHSV of 3744 cc/g/h (see black curve in Figure 4). MDA reactivity evaluation of the as-synthesized Fe-ZSM-5 catalyst to create a spent sample is shown in Figure S2. As seen, the catalyst was fully deactivated after 14 h of MDA reactivity evaluation. Deconvolution of the TPO curve identifies three distinct types of coke with varied oxidation temperatures: a lower-oxidation-temperature coke at 430 °C, so-called soft coke, and two higher-oxidation-temperature cokes at 520 °C and 600 °C, referred to as hard coke and graphitic coke, respectively. Previous studies reported the formation of three types of coke during light alkane conversion on metal-promoted zeolite catalysts, in agreement with our observation of three distinct coke types with varying oxidation temperatures on Fe-ZSM-5 catalysts [24–26]. These coke types include carbidic, polyaromatic, and graphitic carbon, where carbidic carbon originates from carburized metal species formed during catalyst activation [25,27], while polyaromatic coke, composed of heavier aromatic species, results from the polymerization of C_2 and C_6H_6 and exhibits oxidation temperatures between 400 and 600 °C. Graphitic carbon is formed through the deep dehydrogenation of carbon-containing intermediates, characterized by its hydrogen-poor and highly unreactive nature, with a combustion temperature exceeding 500 °C [28]. This agrees well with reports of Mo-zeolite catalysts which also identify three kinds of carbonaceous deposits, attributed to Mo-associated coke as well as aromatic-type coke on the acid sites in Mo-HMCM catalysts [25]. Similarly, the formation of distinct types of coke with varied oxidation temperatures was reported for Mo-HZSM-5 catalysts during MDA, which depended on the coke's location within the zeolite catalysts [26].

In order to identify the impact of the different types of coke types on Fe-ZSM-5 catalytic activity in MDA, samples with controlled amounts of soft, hard, and graphitic coke were prepared via controlled coke burn-off as follows: First, to generate a sample with hard and graphitic coke, a spent (i.e., fully coked) sample was partially regenerated using 20% O_2 in Ar (5 SCCM O_2 and 20 SCCM of Ar) at 425 °C for 15 min. Then, O_2 flow was turned off until the catalyst temperature reached 700 °C, i.e., the catalyst was exposed to the remainder of the temperature ramp in pure nitrogen flow. This procedure was adapted to assure that all catalysts had the same temperature history and only differed in oxidative coke removal. This process selectively eliminated soft coke, yielding a sample with mostly hard and graphitic coke, as confirmed via TPO analysis (see Figure 4, blue curve).

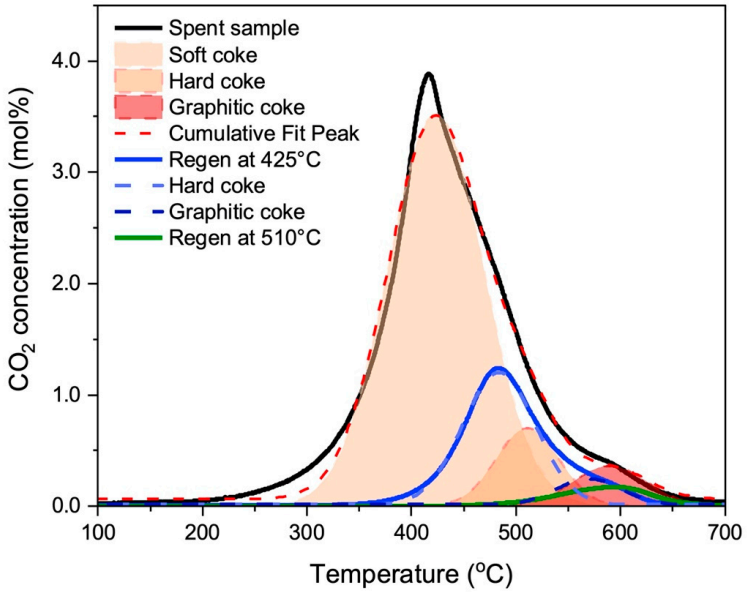

Figure 4. Temperature-programmed oxidation (TPO) analysis of coked catalyst sample deactivated for 14 h. in MDA at 700 °C in a 50:50 CH_4:Ar environment at a WHSV of 3744 cc/g/h (black curve), partially regenerated via oxidation with 20% O_2 in Ar at 425 °C for 15 min (blue curve), and regenerated in 20% O_2 in Ar at 510 °C for 20 min (green curve). These varying regeneration treatments result in the creation of samples with different defined coke distributions for subsequent testing in MDA.

In order to generate a sample with mainly graphitic coke, a fully coked sample was regenerated using 20% O_2 in Ar at 510 °C for 20 min (i.e., slightly higher temperature and longer regeneration time than above), and then O_2 flow was turned off until the catalyst temperature reached 700 °C. This treatment removed both soft and hard coke, resulting in a sample containing only a small amount of residual graphitic coke as again confirmed via TPO analysis (see Figure 4, green curve).

Finally, a third sample was prepared in which all coke was burnt off via oxidation using 20% O_2 in Ar up to 700 °C. This regeneration treatment oxidized all three types of coke (soft, hard, and graphitic coke), thus creating a sample devoid of any coke. This was confirmed by TPO analysis on the sample regenerated at 700 °C (not shown). As expected, no residual coke was detectable in the TPO analysis for this sample. Table 2 summarizes the relative amounts of the three types of coke in these samples.

Table 2. Distributions of various types of coke in spent and coked samples regenerated at 425 °C and 510 °C.

Samples	Integrated Area [a.u.] and Area (%)		
	Soft coke	Hard coke	Graphitic coke
Spent sample	394.4 (84%)	49.8 (10.6%)	25 (5.4%)
Regen at 425 °C	-	103.2 (85.2%)	17.9 (14.8%)
Regen at 510 °C	-		18.49 (100%)

MDA reactivity was evaluated for these samples to correlate the amount and type of coke with catalyst activity. Figure 5 shows the results in terms of methane conversion, benzene selectivity, and benzene concentration versus time-on-stream. (The reactivity of the fully coked sample is not shown, since this catalyst was fully deactivated after 14 h of MDA, as evidenced by the data for the as-synthesized sample in Figure S2.) One can see that the sample containing both hard and graphitic coke (the first sample above, regenerated at

425 °C, shown here again in blue) shows a lower maximum methane conversion of ~1.5% compared to the sample where hard coke was removed (the second sample, regenerated at 510 °C, shown in green), which showed a methane conversion of 5%. Clearly, hard coke removal is critical to recovering catalyst activity via methane conversion. Further burn-off of the graphitic coke (the third sample, regenerated at 700 °C, shown in orange) did not further improve conversion (compare the green and orange curves). This indicates that hard coke is formed and located at the metal site, thus hindering methane activation.

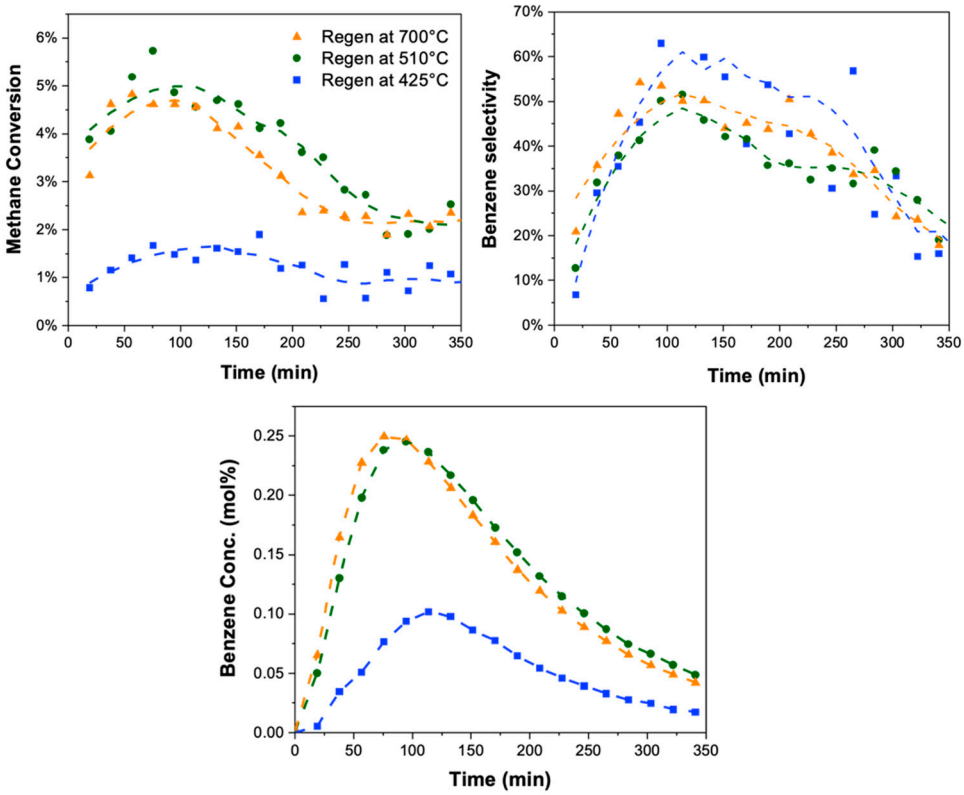

Figure 5. MDA reactivity evaluation (methane conversion, benzene selectivity, and benzene concentration versus time-on-stream) for the three samples after different regeneration procedures (and hence different coke distributions): catalyst containing hard and graphitic coke (regenerated in 20% O_2 in Ar at 425 °C for 15 min, shown in blue); catalyst containing only graphitic coke (regenerated in 20% O_2 in Ar at 510 °C for 20 min, shown in green) and fully regenerated, coke-free catalyst (regenerated in 20% O_2 in Ar till 700 °C, shown in orange). Samples exhibiting hard coke demonstrated reduced methane conversion, suggesting the association of hard coke with the metal sites.

Analyzing benzene selectivity, the removal of soft coke (first sample, regenerated at 425 °C, shown in blue) exhibited the highest benzene selectivity compared to other samples, suggesting soft coke forms at the Brønsted acid sites, hindering the aromatization reaction. Further removing hard coke and, consequently, graphitic coke from the sample (green and orange curves) did not increase benzene selectivity further. Instead, there is a slight decrease, possibly due to the dehydration of Brønsted acid sites (BAS) caused by the local high temperatures during the oxidative burn-off of hard/graphitic coke. The unchanged benzene selectivity following the removal of hard and graphitic coke hence suggests that hard coke is not associated with the BAS, where benzene formation occurs.

2.3. Pyridine FTIR for Identification of Coke on BAS

To further validate these hypotheses and provide direct evidence, pyridine FTIR and H_2 TPR analyses were employed on the coked samples to quantify acid sites and metal sites

in the catalysts, respectively. Since the samples regenerated at 510 °C and 700 °C showed only marginal differences in MDA reactivity, only the sample regenerated at 410 °C and the fully regenerated sample at 700 °C were further examined to differentiate between soft and hard coke on the active sites.

The association of soft coke with the Brønsted acid sites in the zeolite was investigated via pyridine FTIR analysis of the catalyst samples, including the as-synthesized Fe-ZSM-5, in order to quantify the presence of BAS (see Figure 6). Three distinct peaks can be seen within the wavenumber range of 1400–1560 cm^{-1}. The band at 1550 cm^{-1} corresponds to the adsorption of pyridine on Brønsted acid sites (BAS) and is due to the C−C stretching vibration of the pyridinium ion, while the band at 1440 cm^{-1} is characteristic of pyridine bound to Lewis acid sites (LAS); the third band at 1490 cm^{-1} is attributed to pyridine interactions with both LAS and BAS [29].

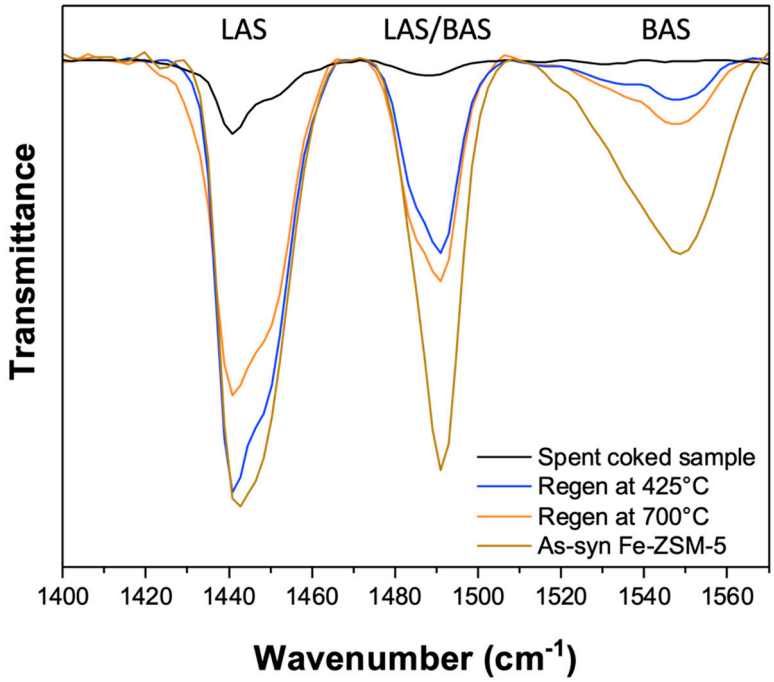

Figure 6. Pyridine FTIR analysis of as-synthesized Fe-ZSM-5 catalyst (shown in brown); fully regenerated, coke−free catalyst (created via oxidative treatment at 700 °C, shown in orange); catalyst containing only hard coke (created via oxidative treatment at 425 °C, shown in blue); and fully spent, coked sample (deactivated for 14 h in MDA at 700 °C, shown in black).

The spent sample (before any coke removal; spectrum shown in black) showed no presence of BAS and only a small signal associated with LAS sites, as expected since coke was blocking the acid sites in this catalyst sample. Upon the removal of soft coke via regeneration at 425 °C (as described above; spectrum shown in blue), the signals indicating both BAS and LAS sites increased, confirming the association of soft coke with both Brønsted and Lewis acid sites. Further removal of both soft and hard coke, resulting in an essentially coke-free sample (spectrum shown in orange), led to only a slight increase in the pyridine adsorption band at 1550 cm^{-1} associated with Brønsted acid sites (BAS). This finding aligns with the reactivity evaluation, which showed only a slight increase in benzene selectivity for this sample possibly due to the oxidation of a small amount of residual soft coke. However, a decrease in the LAS signal was observed which we attribute to the high temperatures locally attained during the oxidative treatment, resulting in the loss of LAS sites due to localized restructuring of the zeolite.

Overall, these results hence confirm our hypothesis and provide direct evidence that soft coke is associated with the acid sites in the Fe-ZSM-5 catalyst.

2.4. H_2 TPR for Identification of Coke on Metal Sites

To validate the association of hard coke with the metal site, H_2 temperature-programmed reduction (TPR) was used as a metal probe reaction to compare the different coked and regenerated catalyst samples with a (metal-free) H-ZSM-5 as the reference and an as-synthesized Fe-ZSM-5 catalyst. The results are shown in Figure 7.

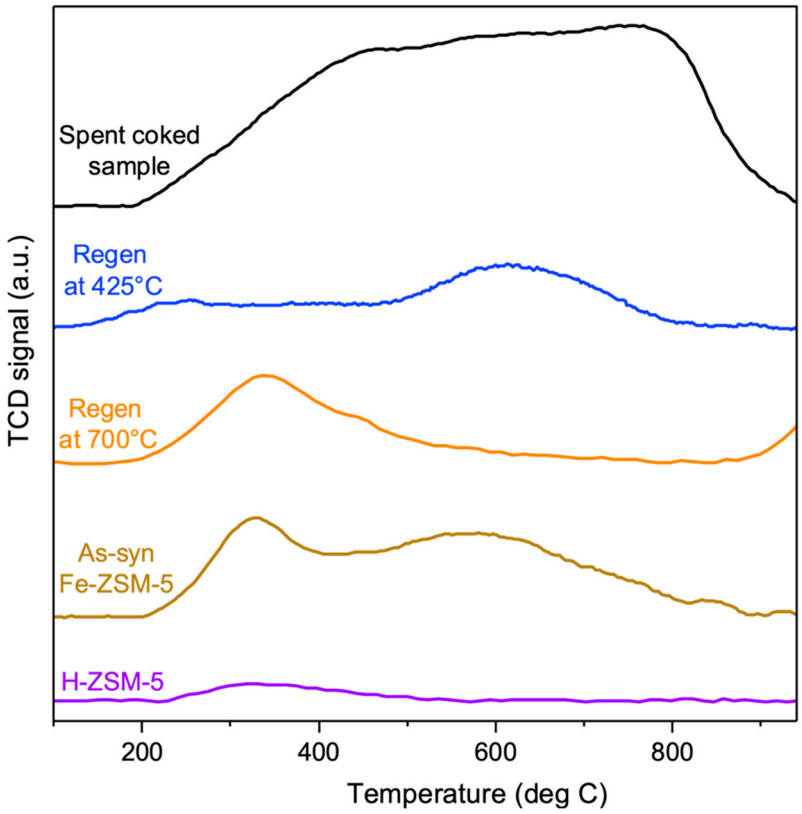

Figure 7. H_2 TPR analysis of H-ZSM-5 (shown in purple); isomorphous substituted as−synthesized Fe-ZSM-5 (shown in brown); fully regenerated, coke-free catalyst (created by removing both soft and hard coke by oxidative treatment at 700 °C, shown in orange); catalyst containing only hard coke (created by removing soft coke by oxidative treatment at 425 °C, shown in blue); and fully spent, coked sample (deactivated for 14 h in MDA at 700 °C, shown in black).

The metal-free zeolite does not show any discernible signal (spectra shown in purple in Figure 7), confirming that any H_2 signal for the other samples must originate from the metal site or coke. The as-synthesized Fe-ZSM-5 catalyst shows pronounced Fe reduction peaks at temperatures of 350 °C and 600 °C, with the peak at a temperature of 350 °C assigned to the reduction of Fe_2O_3 oligomeric clusters in the zeolite framework and the high-temperature peak assigned to the reduction of framework Fe^{3+} to Fe^{2+} [30].

The coked catalyst (containing both soft and hard coke, shown in black) shows a broad peak from 200 to 800 °C, attributed to coke hydrogenation since Fe species (isolated Fe as well as Fe_2O_3 clusters) are inaccessible to hydrogen due to the deposited coke.

As soft coke was burnt off from the spent sample (resulting in a sample with only hard coke, depicted in blue, regen at 425 °C), only one high-temperature peak at 650 °C could be observed which was associated with the framework Fe. Since framework Fe creates BAS, this aligns with our earlier observation that the elimination of soft coke makes BAS sites available. Virtually no signal attributed to Fe_2O_3 clusters at the lower temperature (350 °C) was observed after the removal of soft coke, confirming that soft coke was not associated with these metal sites.

Further removal of hard coke (resulting in a fully regenerated, coke-free sample, depicted in orange) revealed only one low-temperature reduction peak at 350 °C, associated

with Fe_2O_3 clusters. Comparing the orange (regen at 700 °C) and blue curves (regen at 425 °C), it is evident that the removal of hard coke amplifies the signal from the Fe_2O_3 clusters compared to the sample which contains hard coke, indicating the association of hard coke with these Fe_2O_3 sites in the catalyst. In other words, only upon the oxidation of hard coke do Fe_2O_3 sites become accessible, leading to the appearance of signals in the H_2 TPR spectra at 350 °C. This is consistent with the MDA reactivity evaluation, where the removal of hard coke from the metal sites increased methane conversion (in accordance with the reaction mechanism). However, no high-temperature peak associated with the framework Fe peak was observed in the fully regenerated sample at 700 °C. This indicates that the oxidative treatment, which is highly exothermic and hence raises local temperatures of the catalyst during coke burn-off, causes the framework Fe to bleed out and transform into Fe_2O_3 clusters, as reported before [30].

Figure 8 summarizes again schematically the formation of different types of coke (soft versus hard coke) on active sites—metal versus Brønsted acid sites—within the Fe-ZSM-5 catalyst: hard coke is formed predominantly on the metal sites, resulting in a loss of catalyst activity, while soft coke is formed predominantly on the Brønsted acid sites of the zeolite, lowering benzene selectivity.

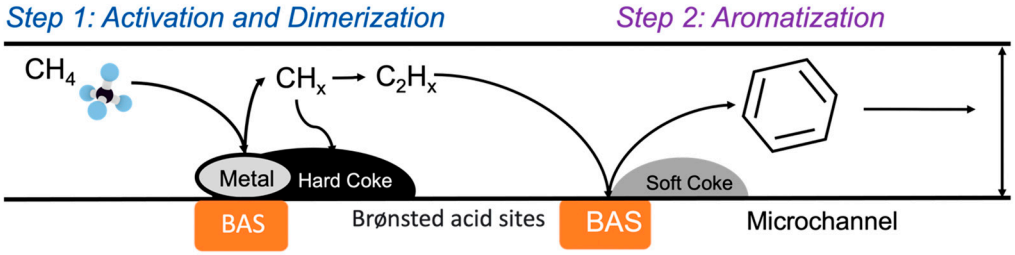

Figure 8. Schematic illustrating the formation of different types of coke (soft versus hard coke) on active sites.

2.5. Regeneration Using CO_2

Both the FTIR characterization (Figure 6) and the H_2-TPR (Figure 7) of the catalysts after regeneration suggested that the high exothermicity of the coke burn-off using oxygen was destructive for the catalyst framework by causing the bleed-out of the metal phase. This is further supported by the UV-Vis analysis of as-synthesized and O_2-regenerated samples (Figure S5) which confirms the increased aggregation of Fe species. Therefore, we explored the use of CO_2 as an alternative, mild oxidant. In contrast to the exothermal coke burn-off using oxygen, the regeneration with CO_2 is endothermal and should hence avoid local hot spots during burn-off.

Furthermore, our above-discussed results showed an association of hard coke with the metal site, making the removal of hard coke during the regeneration process critical in order to restore catalyst activity. Since CO_2 is a comparatively weak ("mild") oxidant, this requires high regeneration temperatures. Spent samples, deactivated in MDA at 700 °C for 14 h. at a WHSV of 936 cc/g/h in 50%CH_4 in Ar flow, were hence subjected to CO_2 regeneration (25 SCCM) at temperatures of 830 °C and 860 °C. Subsequently, TPO (using 20% O_2 in Ar) was again used to elucidate the distribution of coke on the catalyst. The results are shown in Figure 9.

Consistent with previous findings, three types of coke were observed on the spent sample: soft coke, hard coke, and graphitic coke. However, the distribution of coke differed from the previous sample, with more hard and graphitic coke formed on these catalysts (cp. Figure 4). This difference can be attributed to the lower WHSV of 936 cc/g/h utilized during the MDA reaction, as opposed to the 3744 cc/g/h employed in previous experiments, which resulted in increased contact times of the reactant feed (i.e., CH_4) in the reactor and hence increased the formation of hard and graphitic coke. (The additional peak at 300 °C is an experimental artifact due to the glass wool used for catalyst packing in the

reactor. The glass wool contains a starch binder, which oxidizes to produce the CO_2 peak during the TPO analysis. This peak was absent in the previous sample, as the binder had been burnt off before those experiments.)

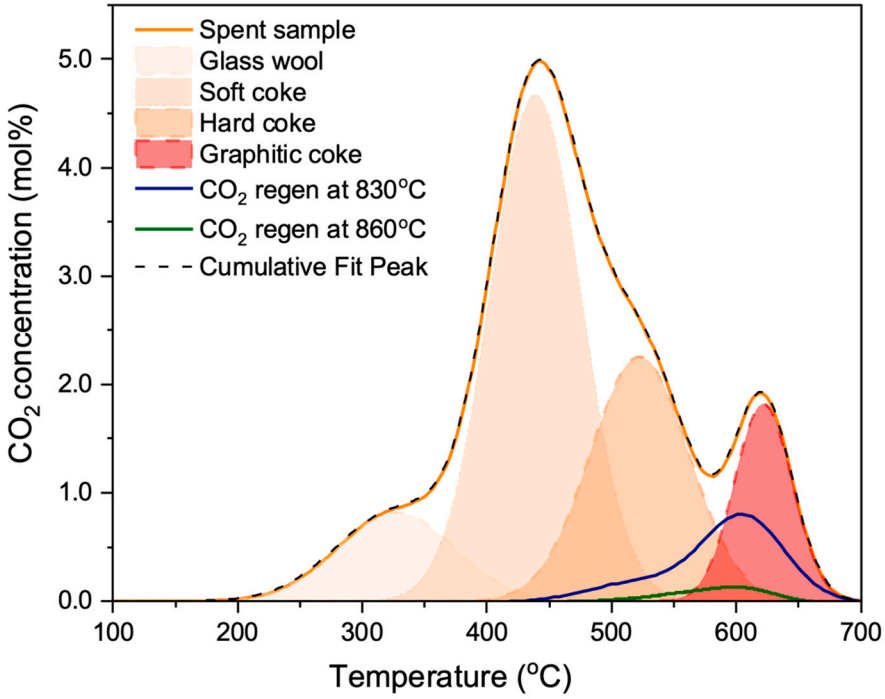

Figure 9. Temperature-programmed oxidation (TPO) on a spent coked sample (deactivated via MDA reaction at 700 °C for 14 h at WHSV of 936 cc/g/h in 50%CH_4 in Ar flow), a CO_2-regenerated spent sample at 830 °C for 30 min, and a CO_2-regenerated spent sample at 860 °C for 30 min. TPO analysis revealed that CO_2 preferentially removes soft coke, while hard coke persists until 830 °C.

Consistent with expectations, CO_2—as a soft oxidant—predominantly removed soft coke formed at the Brønsted acid sites. CO_2 regeneration at 830 °C (shown in blue) facilitated the removal of soft coke, but only a partial removal of hard coke. Further increasing temperature to 860 °C facilitated a more complete removal of coke, including hard coke (shown in green). Based on our above results, methane conversion and benzene concentration should hence increase with increasing regeneration temperature.

This was verified via MDA reactivity evaluations with catalysts regenerated at different temperatures ranging from 800 °C to 860 °C. First, the spent sample was obtained through deactivation via MDA at 700 °C for 14 h with a WHSV of 936 cc/g/h and a 50% CH_4 in argon flow. Then, the spent samples underwent CO_2 regeneration at temperatures of 800 °C, 830 °C and 860 °C, respectively, with a flow rate of 25 SCCM. MDA reactivity evaluations were performed on these CO_2-regenerated samples at varied temperatures. Figure 10 shows the results of MDA reactivity performance in terms of methane conversion, benzene selectivity, and benzene concentration.

The CO_2-regenerated sample at 800 °C displayed the lowest methane conversion compared to samples regenerated at higher temperatures, indicating ineffective oxidation of hard coke at metal sites, hindering methane activation in the regenerated catalyst. Furthermore, the lower methane conversion observed in the CO_2-regenerated sample compared to the O_2-regenerated sample (see Figure S3) confirms CO_2's inability to oxidize hard coke at the metal site. Additionally, UV-Vis analysis conducted on the CO_2-regenerated sample at various temperatures (see Figure S4) provides further evidence of the presence of coke even after the CO_2 regeneration treatment at 800 °C.

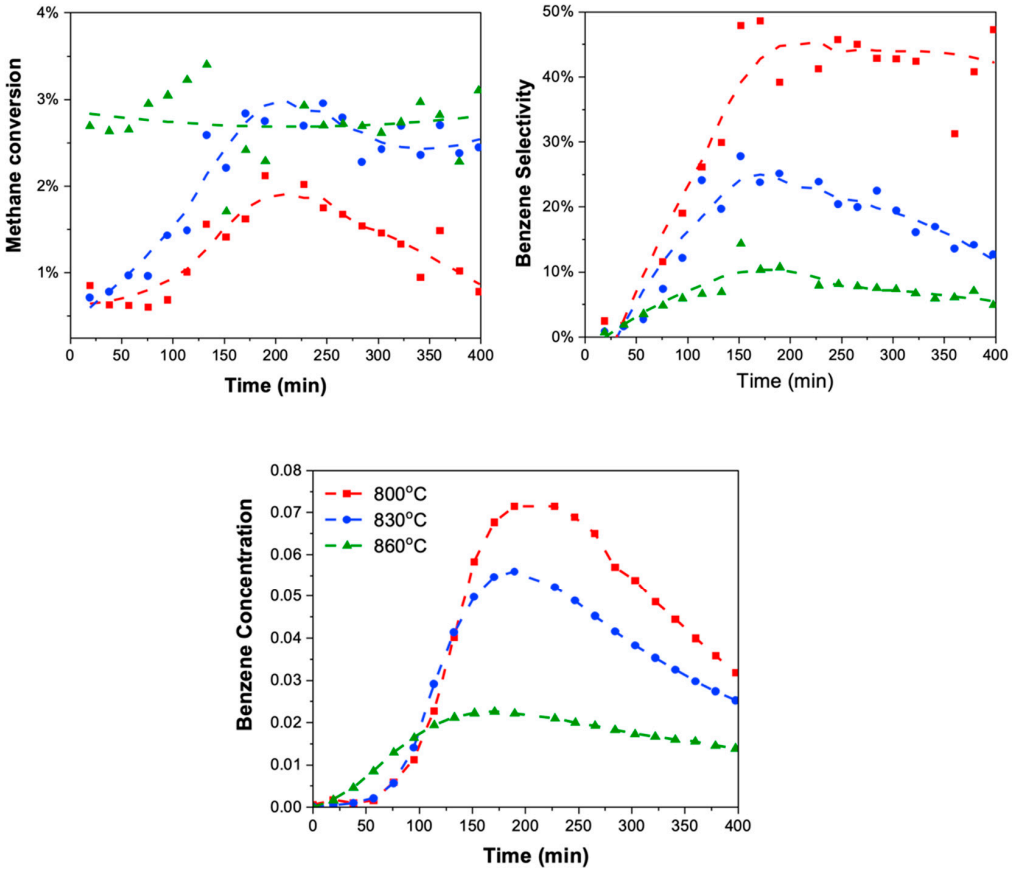

Figure 10. MDA reactivity performance (conversion, benzene selectivity, and overall concentration of benzene) on CO_2-regenerated spent samples at varying temperatures: 800 °C (shown in red), 830 °C (shown in blue), and 860 °C (shown in green). Spent samples were deactivated via MDA reaction at 700 °C for 14 h. at a WHSV of 3750 cc/g/h in 50%CH_4 in Ar flow. Increasing the CO_2 regeneration temperature from 800 °C to 860 °C led to enhanced methane conversion, although with a decrease in benzene selectivity, attributable to catalyst deactivation.

With an increase in CO_2 regeneration temperature from 800 °C to 860 °C, methane conversion increased as anticipated, attributed to the removal of hard coke at the metal site. However, a concomitant decrease in benzene selectivity was observed, reducing the overall benzene yield despite efficient coke removal. Considering the elevated temperatures required for CO_2 regeneration, we hypothesized that the diminished benzene selectivity (and thus yield) could be linked to the deactivation of the catalyst caused by either the collapse of the ZSM-5 structure or Brønsted acid dehydration under these conditions. Thus, the effect of higher temperatures was examined on the structural stability of the zeolite catalyst as well as the Brønsted acid sites via XRD and pyridine FTIR analysis, respectively.

Figure 11 shows the X-ray diffraction (XRD) analysis for the as-synthesized, fully deactivated (coked) sample after MDA reaction at 700 °C for 14 h. under 50%CH_4 in Ar flow, along with the same spent sample thermally treated in 0.5 SCCM of Ar flow at 800 °C, 830 °C, and 860 °C. All samples show diffraction peaks at 7.9° and 8.9°, along with a characteristic triplet at 23.5° in the XRD spectra, indicating the presence of a crystalline MFI structure. The as-synthesized sample displays the highest peak intensity. A decrease in intensity was observed for the spent samples, indicating a decrease in crystallinity due to exposure to the reaction temperature of 700 °C for 14 h.

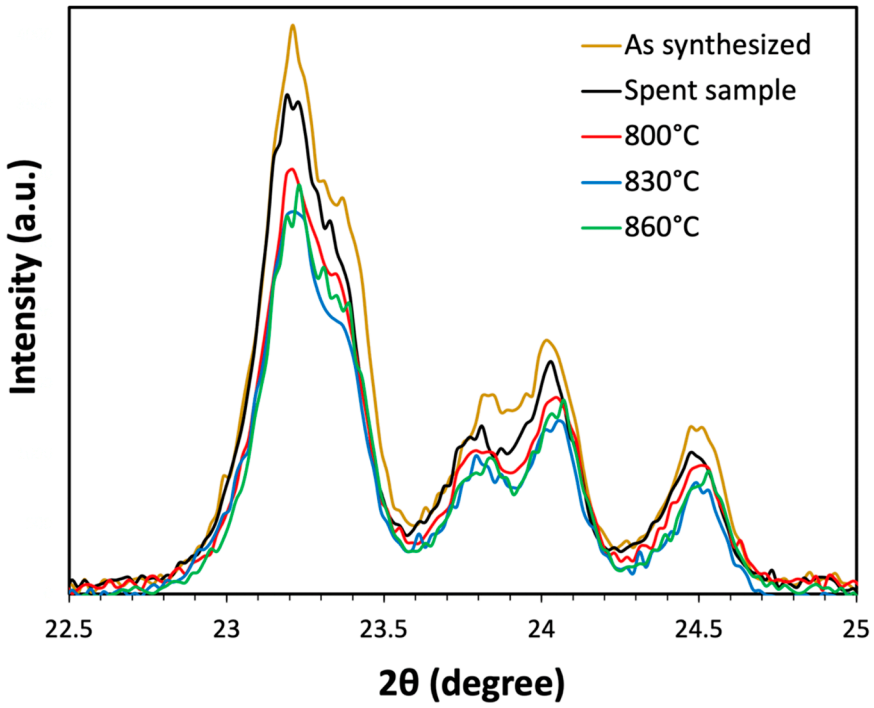

Figure 11. X-ray diffraction (XRD) analysis was conducted on the as-synthesized sample, spent sample, and spent sample thermally treated at temperatures ranging from 800 °C to 860 °C for 30 min in 0.5 SCCM of Ar flow.

Further reduction in peak intensities was observed after the thermal treatment of this spent sample at higher temperatures, indicating a further loss of crystallinity, albeit the loss seemed largely independent of the precise temperature in the 800–860 °C range. Notably, even at the maximum temperature of 860 °C, discernible MFI peaks were observed in the XRD spectra, indicating the preservation of the zeolite structure under these elevated temperature conditions, at least over the duration of the thermal treatment.

This suggests that a loss of crystallinity was unlikely to be causing the observed decline in benzene selectivity at elevated temperatures. Therefore, a potential loss of Brønsted acid sites via dehydration was probed next, again using pyridine FTIR analysis on an as-synthesized sample, thermally treated in a 0.5 SCCM Ar flow at 700 °C for 14 h (i.e., mimicking the thermal exposure during MDA reaction), followed by heating to 800 °C, 830 °C, and 860 °C at a ramp rate of 5 °C/min, and holding for 30 min. The pyridine FTIR analysis of these three thermally treated samples is shown in Figure 12.

With the increasing temperature of the thermal treatment from 800 °C to 860 °C, the signal at the wavenumber of 1550 cm^{-1}, associated with Brønsted acid sites, decreases and the LAS peak (at 1440 cm^{-1}) increases, indicating the conversion of BAS to LAS. This can be explained again by a bleed-out of aluminum or iron atoms from the zeolite crystal lattice, removing the associated BAS and generating additional iron species outside the lattice structure, characterized by their Lewis acidic properties [31]. This hence confirms that the decrease in benzene selectivity is caused by a loss of BAS, the active sites for benzene formation, due to the insufficient thermal stability of the metal substituent in the zeolite lattice.

Overall, although coke oxidation using CO_2 is an endothermic process and therefore avoids the well-known local temperature maxima during oxidation, the weakly oxidizing nature of CO_2 requires elevated temperatures to oxidize hard coke for the recovery of metal sites which are crucial for methane activation. However, these elevated temperatures result in catalyst deactivation due to the loss of Brønsted acid sites (BAS), negating the desired "mild oxidation" target. This result hence underscores the importance of a durable and resilient catalyst when employing CO_2 regeneration.

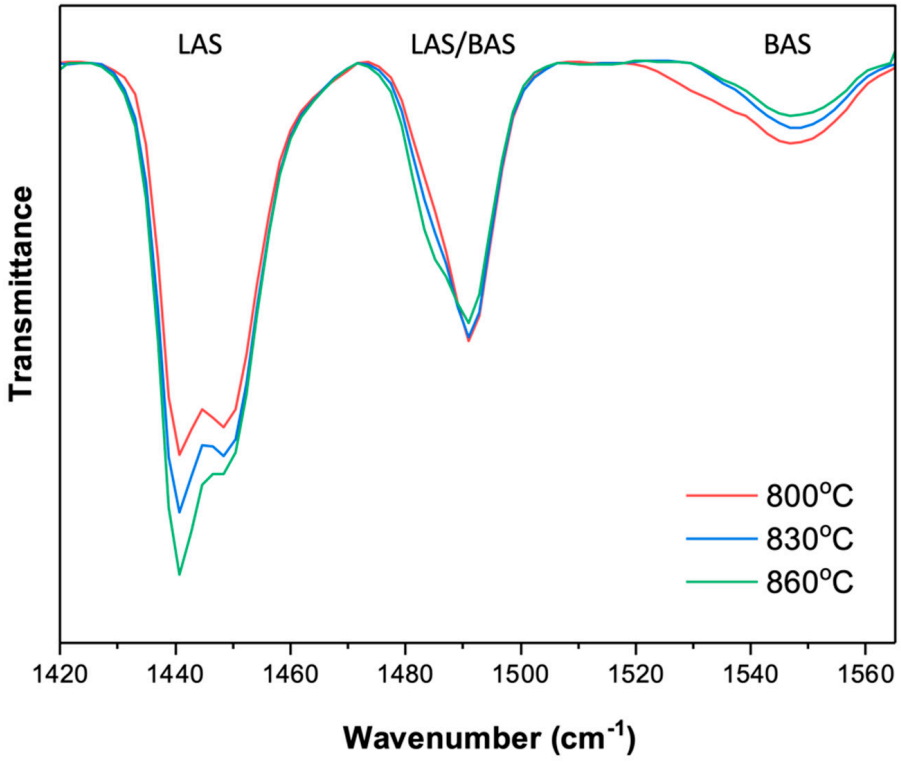

Figure 12. Pyridine FTIR analysis of as−synthesized Fe-ZSM-5 and thermally treated Fe-ZSM-5 at varying temperatures ranging from 700 °C to 860 °C for 30 min.

3. Experimental Section

3.1. Catalyst Synthesis

H-(Fe)-ZSM-5 (Isomorphous Substitution) Synthesis

Typically, 0.295 g of iron nitrate nonahydrate ($Fe(NO_3)_3.9H_2O$), corresponding to 2 wt.% of Fe loading, was added to 24.26 mL of deionized water. Then, 6.94 g of tetraethyl orthosilicate (TEOS, >99.0%) was added dropwise to the above mixture and stirred for 3 h. A second mixture was prepared by combining 0.312 g of $Al(NO_3)_3{\cdot}9H_2O$ (>98%, Sigma Aldrich, St. Louis, MO, USA), 3.387 g of tetrapropylammonium hydroxide (TPAOH) aqueous solution (1 M in H_2O, Sigma Aldrich), and 0.266 g of NaOH (pellets, 98%). TPAOH acted as a structure-directing agent in the synthesis. The first mixture was then added dropwise to the second mixture, stirred for 18 h at room temperature, transferred to a Teflon-lined stainless-steel autoclave, and hydrothermally treated at 175 °C for 24 h under rotation. The obtained Na-ZSM-5 was washed thoroughly with deionized water and dried overnight, followed by calcination at 550 °C in air for 10 h. Na-ZSM-5 was further converted to H-Fe-ZSM-5 by ion exchange with an aqueous NH_4NO_3 solution at 85 °C for 15 h. Finally, the material was dried at 80 °C and calcined at 500 °C in air for 5 h.

3.2. Material Characterization

3.2.1. X-ray Diffraction (XRD)

The catalysts were characterized by X-ray diffraction (XRD) using monochromatic Cu radiation at the wavelength of 1.54 Å. to determine its crystal structure (Bruker D8 Discover, Billerica, MA, USA). The beam voltage and current used were 40 kV and 40 mA, respectively. Analysis was performed for scanning angles (2θ) ranging from 5° to 50° with increments of 0.02° at a scanning speed of 0.5 s/step.

3.2.2. Scanning Electron Microscopy and Energy-Dispersive X-ray Analysis (SEM and EDX)

A Zeiss SIGMA VP field emission scanning electron microscope (SEM) at a beam voltage of 3 kV was used to determine material morphology (Zeiss, Oberkochen, Germany). Samples were deposited on carbon tape for SEM morphology analysis. The elemental composition of catalysts was determined by energy-dispersive X-ray spectroscopy (EDX) with a total collection count of 50,000 at a beam voltage of 15 Kv (Zeiss, Oberkochen, Germany).

3.2.3. Nitrogen Sorption Measurements (BET)

Nitrogen adsorption/desorption analysis was performed using a surface area and porosity analyzer (Micromeritics, ASAP 2020, Norcross, GA, USA) at 77 °K. Before analysis, samples were degassed for 24 h under 10 um Hg vacuum pressure and 300 °C temperature to desorb moisture and impurities from the zeolite sample. Specific surface areas were determined using the Brunauer–Emmett–Teller (BET) method.

3.2.4. UV-Vis Diffuse Reflectance Spectroscopy (UV-Vis DRS)

UV-Vis Diffuse Reflectance Spectroscopy (UV-Vis DRS) measurement was conducted on the Fe-ZSM-5 sample using a Lambda 750 UV/Vis/NIR microspectrophotometer with a diffuse reflectance accessory to determine the iron speciation (PerkinElmer, Shelton, CT, USA). Barium sulfate was used to dilute the sample, and the ratio of sample to barium sulfate weight was maintained at 1:4. The instrument background was eliminated by subtracting a spectrum obtained from a blank run involving pure barium sulfate. Variation of reflectance with wavelength was obtained from the UV-Vis spectrometer. The concentration of Fe species was obtained by calculating the Kubelka–Munk function, $F(R)$ which correlates the analyte concentration (Fe species) and its adsorption. It is given as:

$$F(R) = \frac{(1-R)^2}{2R} = \frac{2.303\epsilon C}{S} \quad (1)$$

where reflectance (R) is calculated as $R_{sample}/R_{reference}$, C is the concentration, S is the scattering coefficient, and ϵ is the absorptivity. The obtained $F(R)$ spectra were deconvoluted into sub-bands using the Gaussian function in the OriginLab software (Origin 2024). The distribution of Fe species was determined based on the percentage area of the absorption sub-bands in $F(R)$ function [32].

3.2.5. Pyridine Diffuse Reflectance Fourier Transform Infrared Spectroscopy (DRIFTS)

To investigate the Brønsted acid sites, in situ Diffuse Reflectance Fourier Transform Infrared spectroscopy (DRIFTS) was carried out using pyridine as a probe molecule. The experiments employed a liquid nitrogen-cooled MCT detector (Bruker Vertex-70LS FTIR, Billerica, MA, USA) and an environmentally controlled PIKE DiffuseIR cell with KBr windows at ambient pressure. The measurements were conducted on as-synthesized and post-reaction (i.e., coked) Fe-ZSM-5 samples. Spectra were acquired at room temperature between 1420 and 1560 cm^{-1} with a resolution of 4 cm^{-1}. The sample chamber was purged with N_2 (20 SCCM), and a background scan was recorded. Subsequently, pyridine vapors were introduced into the chamber by flowing N_2 through liquid pyridine, and pyridine–DRIFTS spectra were collected until no discernible change in the spectrum was observed. Another round of N_2 purge was initiated, and pyridine–DRIFTS data were recorded until stability in the spectra was achieved.

3.2.6. Hydrogen Temperature-Programmed Reduction (H_2 TPR)

H_2-TPR was conducted to identify metal species (Fe) in Fe-ZSM-5 samples by evaluating their reducibility with H_2. A Micromeritics Chemisorb 2750 system equipped with a thermal conductivity detector (TCD) was employed for this experiment (Micromeritics, Norcross, GA, USA). Each H_2-TPR experiment utilized 0.1 g of sample (Micromeritics,

Norcross, GA, USA). The sample was heated at a rate of 10 °C per minute to 1000 °C in a flow of 20 SCCM of 5% H_2 (in argon). To eliminate water vapor, a cold trap filled with an acetone–dry ice mixture was positioned downstream of the reactor before the TCD detector.

3.3. Reactivity Evaluation

Reactivity tests were carried out in a fixed-bed reactor at 700 °C and atmospheric pressure. Typically, a quartz tubular reactor (ID 5 mm) was filled with 0.1 g of Fe-ZSM-5 catalyst between two plugs of quartz wool. The catalyst was first calcined in air at 500 °C for 20 min and then heated to the desired reaction temperature (700 °C) under argon flow. After temperature equilibration, 50 vol.% methane (6.25 SCCM) in argon was introduced. Weight hourly space velocity (WHSV) of the gas feed was kept constant at 3750 (cc/g/h) in all experiments. The effluent gas was analyzed by gas chromatography equipped with thermal conductivity (TCD) and flame ionization detectors (FID), (Agilent 7890B GC, Santa Clara, CA, USA). Ar gas was used as an internal standard. C_2 products (ethylene and ethane) and benzene were the only gaseous products identified across all reported reaction conditions. Since methane conversion and benzene selectivity constitute sensitive probes for the active sites in the catalyst, only these two quantities are reported here. Methane conversion (X_{CH_4}) and benzene selectivity (S) were calculated using Equations (2) and (3), where n_j represents the number of moles of species j.

$$X_{CH_4} = \frac{n_{CH_4,\,in} - n_{CH_4,\,out}}{n_{CH_4,\,in}} \tag{2}$$

$$S_{C_6H_6} = \frac{6 \times n_{C_6H_6,\,out}}{n_{CH_4,\,in} - n_{CH_4,\,out}} \tag{3}$$

3.4. Regeneration of Spent Sample Using CO_2 or 20% O_2 in Ar

Coked catalysts, after MDA experimental runs, were regenerated using 25 SCCM of CO_2 or 20% O_2 in Ar at varied temperatures ranging from 800 °C to 860 °C, respectively, to study the effect of the type of regeneration on MDA reactivity performance. Regeneration temperature was ramped up to the specified temperature (with a ramp rate of 5 °C/min) and maintained at that temperature for 30 min.

3.5. Carbon Deposition Analysis

Temperature-programmed oxidation (TPO) was performed to determine the amount and type of carbonaceous species present in the spent samples after reactivity and regeneration tests. Catalyst samples were oxidized in 20% O_2 in argon (5 SCCM oxygen and 20 SCCM of argon mixture) flow while ramping the temperature to 1000 °C at 5 °C/min. Mass spectrometry (Pfeiffer Vacuum Omnistar GSD 320, Aßlar, Germany) was used to monitor the carbon burn-off process.

4. Conclusions

Coke formation methane dehydro-aromatization (MDA) presents a major challenge for process development. While coke formation and regeneration have been studied in significant depth for Mo-ZSM-5 catalysts, the present study extended such investigations onto the less-studied Fe-ZSM-5 catalysts for MDA.

Our study identified three types of coke formed during MDA over these catalysts: soft coke, which is highly reactive and hence easily oxidized, and hard/graphitic coke, which are deeply dehydrogenated and hence less reactive, requiring higher oxidation temperatures. By analyzing coked samples containing carefully controlled fractions of soft and hard coke using reactive studies, XRD, H_2-TPR, and pyridine FTIR, we were able to show that hard coke deactivates the metal sites, leading to a loss of methane conversion (i.e., catalyst activity), and suggesting that this coke is the result of deep dehydrogenation of methane during the activation of CH_4 on the metal site. In contrast, soft coke was located

on the Brønsted acid sites, causing a loss of benzene selectivity, suggesting that this coke is formed via polymerization and partial dehydrogenation of aromatics.

Aiming to avoid damage to the zeolite structure during oxygen-mediated regeneration, we also investigated the use of CO_2 as an alternative, mild oxidant. However, despite elevated regeneration temperatures, CO_2 was only able to partially restore activity by oxidizing soft coke at the Brønsted acid sites (BAS) but could not oxidize hard coke at the metal sites, thus failing to recover methane activation in the regenerated catalyst. A further increase in temperature to improve the efficiency of coke removal caused a loss of BAS from the catalyst and hence a loss of selectivity. Hence, while the use of CO_2 as a mild oxidant is conceptually an interesting regeneration approach, it clearly requires more robust catalyst systems or the use of alternate energy systems that deliver the heat of regeneration more efficiently and directly to the reactive site. Microwave energy, which is known to interact strongly with carbonaceous species [33,34] and has been shown to create metal hot spots [24,35], may be well suited for the targeted removal of hard coke at metal sites and hence improve overall regeneration efficiency.

Overall, this study provides new insights into coke formation and regeneration during MDA on Fe-ZSM-5 catalysts and hence adds to the body of knowledge that can inform the development of more efficient regeneration procedures in order to render MDA an industrially viable process.

Supplementary Materials: The following supporting information can be downloaded at: https://www.mdpi.com/article/10.3390/catal14050292/s1, Figure S1: N_2 adsorption–desorption analysis of as-synthesized 2 wt.% Fe-ZSM-5. Figure S2: MDA reactivity evaluation of as-synthesized Fe-ZSM-5. Figure S3: MDA reactivity evaluation of CO_2 and 20% O_2 in Ar-regenerated 2 wt.%Fe-ZSM-5 spent catalyst. Figure S4: UV-Vis analysis of as-synthesized Fe-ZSM-5 catalyst, O_2-regenerated and CO_2-regenerated catalyst. Figure S5: UV-Vis analysis of as-synthesized Fe-ZSM-5 catalyst and O_2-regenerated catalyst to determine Fe species distribution.

Author Contributions: Conceptualization, G.V. and S.K.; methodology, S.K. and G.V.; validation, S.K. and G.V.; formal analysis, S.K.; investigation, S.K.; resources, G.V.; data curation, S.K.; writing—original draft preparation, S.K.; writing—review and editing, G.V. and S.K.; visualization, G.V. and S.K.; supervision, G.V.; project administration, G.V.; funding acquisition, G.V. All authors have read and agreed to the published version of the manuscript.

Funding: This work was supported by the US Department of Energy through AICHE RAPID under Contract DEEE0007888-6-7.

Data Availability Statement: The raw data supporting the conclusions of this article will be made available by the authors on request.

Acknowledgments: The authors thank the Nanoscale Fabrication and Characterization Facilities (NFCF) and Paul Leu (University of Pittsburgh) for support in materials characterization.

Conflicts of Interest: The authors declare no conflicts of interest.

References

1. Yung, M.M.; Starace, A.K.; Griffin, M.B.; Wells, J.D.; Patalano, R.E.; Smith, K.R.; Schaidle, J.A. Restoring ZSM-5 Performance for Catalytic Fast Pyrolysis of Biomass: Effect of Regeneration Temperature. *Catal. Today* **2019**, *323*, 76–85. [CrossRef]
2. Heracleous, E.; Pachatouridou, E.; Hernández-Giménez, A.M.; Hernando, H.; Fakin, T.; Paioni, A.L.; Baldus, M.; Serrano, D.P.; Bruijnincx, P.C.A.; Weckhuysen, B.M.; et al. Characterization of Deactivated and Regenerated Zeolite ZSM-5-Based Catalyst Extrudates Used in Catalytic Pyrolysis of Biomass. *J. Catal.* **2019**, *380*, 108–122. [CrossRef]
3. Pinard, L.; Ayoub, N.; Batiot-Dupeyrat, C. Regeneration of a Coked Zeolite via Nonthermal Plasma Process: A Parametric Study. *Plasma Chem. Plasma Process.* **2019**, *39*, 929–936. [CrossRef]
4. Astafan, A.; Sachse, A.; Batiot-Dupeyrat, C.; Pinard, L. Impact of the Framework Type on the Regeneration of Coked Zeolites by Non-Thermal Plasma in a Fixed Bed Dielectric Barrier Reactor. *Catalysts* **2019**, *9*, 985. [CrossRef]
5. Vogt, E.T.C.; Fu, D.; Weckhuysen, B.M. Carbon Deposit Analysis in Catalyst Deactivation, Regeneration, and Rejuvenation. *Angew. Chem. Int. Ed.* **2023**, *62*, e202300319. [CrossRef]
6. Ochoa, A.; Bilbao, J.; Gayubo, A.G.; Castaño, P. Coke Formation and Deactivation during Catalytic Reforming of Biomass and Waste Pyrolysis Products: A Review. *Renew. Sustain. Energy Rev.* **2020**, *119*, 109600. [CrossRef]

7. Díaz, M.; Epelde, E.; Valecillos, J.; Izaddoust, S.; Aguayo, A.T.; Bilbao, J. Coke Deactivation and Regeneration of HZSM-5 Zeolite Catalysts in the Oligomerization of 1-Butene. *Appl. Catal. B* **2021**, *291*, 120076. [CrossRef]
8. Hita, I.; Mohamed, H.O.; Attada, Y.; Zambrano, N.; Zhang, W.; Ramírez, A.; Castaño, P. Direct Analysis at Temporal and Molecular Level of Deactivating Coke Species Formed on Zeolite Catalysts with Diverse Pore Topologies. *Catal. Sci. Technol.* **2023**, *13*, 1288–1300. [CrossRef]
9. Cheng, M.; Cruchade, H.; Pinard, L.; Dib, E.; Liu, H.; Wang, J.; Liu, X.; Yan, Z.F.; Qin, Z.; Mintova, S. Coke Relocation and Mo Immobilization in Donut-Shaped Mo/HZSM-5 Catalysts for Methane Dehydroaromatization. *J. Mater. Chem. A* **2023**, *11*, 24991–24998. [CrossRef]
10. Kosinov, N.; Uslamin, E.A.; Coumans, F.J.A.G.; Wijpkema, A.S.G.; Rohling, R.Y.; Hensen, E.J.M. Structure and Evolution of Confined Carbon Species during Methane Dehydroaromatization over Mo/ZSM-5. *ACS Catal.* **2018**, *8*, 8459–8467. [CrossRef]
11. Rahman, M.; Infantes-Molina, A.; Hoffman, A.S.; Bare, S.R.; Emerson, K.L.; Khatib, S.J. Effect of Si/Al Ratio of ZSM-5 Support on Structure and Activity of Mo Species in Methane Dehydroaromatization. *Fuel* **2020**, *278*, 118290. [CrossRef]
12. dos Santos, L.T.; Santos, F.M.; Silva, R.S.; Gomes, T.S.; Esteves, P.M.; Pimenta, R.D.M.; Menezes, S.M.C.; Chamberlain, O.R.; Lam, Y.L.; Pereira, M.M. Mechanistic Insights of CO_2-Coke Reaction during the Regeneration Step of the Fluid Cracking Catalyst. *Appl. Catal. A Gen.* **2008**, *336*, 40–47. [CrossRef]
13. Qingli, X.; Peng, F.; Wei, Q.; Kai, H.; Shanzhi, X.; Yongjie, Y. Catalyst Deactivation and Regeneration during CO_2 Reforming of Bio-Oil. *Int. J. Hydrog. Energy* **2019**, *44*, 10277–10285. [CrossRef]
14. de Mello, L.F.; Pimenta, R.D.M.; Moure, G.T.; Pravia, O.R.C.; Gearhart, L.; Milios, P.B.; Melien, T. A Technical and Economical Evaluation of CO_2 Capture from FCC Units. In *Energy Procedia*; Elsevier: Amsterdam, The Netherlands, 2009; Volume 1, pp. 117–124.
15. Zhou, J.; Zhao, J.; Zhang, J.; Zhang, T.; Ye, M.; Liu, Z. Regeneration of Catalysts Deactivated by Coke Deposition: A Review. *Chin. J. Catal.* **2020**, *41*, 1048–1061. [CrossRef]
16. Cruchade, H.; Medeiros-Costa, I.C.; Nesterenko, N.; Gilson, J.P.; Pinard, L.; Beuque, A.; Mintova, S. Catalytic Routes for Direct Methane Conversion to Hydrocarbons and Hydrogen: Current State and Opportunities. *ACS Catal.* **2022**, *12*, 14533–14558. [CrossRef]
17. Sim, T.J.; Shim, J.; Lee, G.; Ko, Y.S.; Choi, J. Tailored Chemical Modification of ZSM-5 Zeolite Supports for Mo-Based Catalysts Optimized for Methane Dehydroaromatization: Hydrothermal Dealumination Was Key to Improving the Selectivity of Desired Aromatic Compounds. *Catal. Today* **2024**, *425*, 114357. [CrossRef]
18. Beuque, A.; Hao, H.; Berrier, E.; Batalha, N.; Sachse, A.; Paul, J.F.; Pinard, L. How Do the Products in Methane Dehydroaromatization Impact the Distinct Stages of the Reaction? *Appl. Catal. B* **2022**, *309*, 121274. [CrossRef]
19. Pérez-Ramírez, J.; Mul, G.; Kapteijn, F.; Moulijn, J.A.; Overweg, A.R.; Doménech, A.; Ribera, A.; Arends, I.W.C.E. Physicochemical Characterization of Isomorphously Substituted FeZSM-5 during Activation. *J. Catal.* **2002**, *207*, 113–126. [CrossRef]
20. Lai, Y.; Veser, G. The Nature of the Selective Species in Fe-HZSM-5 for Non-Oxidative Methane Dehydroaromatization. *Catal. Sci. Technol.* **2016**, *6*, 5440–5452. [CrossRef]
21. Bordiga, S.; Buzzoni, R.; Geobaldo, F.; Lamberti, C.; Giamello, E.; Zecchina, A.; Leofanti, G.; Petrini, G.; Tozzola, G.; Vlaic, G. Structure and Reactivity of Framework and Extraframework Iron in Fe-Silicalite as Investigated by Spectroscopic and Physicochemical Methods. *J. Catal.* **1996**, *158*, 486–501. [CrossRef]
22. Pérez-Ramírez, J.; Kumar, M.S.; Brückner, A. Reduction of N_2O with CO over FeMFI Zeolites: Influence of the Preparation Method on the Iron Species and Catalytic Behavior. *J. Catal.* **2004**, *223*, 13–27. [CrossRef]
23. Groen, J.C.; Brückner, A.; Berrier, E.; Maldonado, L.; Moulijn, J.A.; Pérez-Ramírez, J. Iron Site Modification upon Alkaline Treatment of Fe-ZSM-5 Zeolites-Opportunities for Improved N_2O Decomposition Activity. *J. Catal.* **2006**, *243*, 212–216. [CrossRef]
24. Deng, Y.; Bai, X.; Abdelsayed, V.; Shekhawat, D.; Muley, P.D.; Karpe, S.; Mevawala, C.; Bhattacharyya, D.; Robinson, B.; Caiola, A.; et al. Microwave-Assisted Conversion of Methane over H-(Fe)-ZSM-5: Evidence for Formation of Hot Metal Sites. *Chem. Eng. J.* **2021**, *420*, 129670. [CrossRef]
25. Ma, D.; Wang, D.; Su, L.; Shu, Y.; Xu, Y.; Bao, X. Carbonaceous Deposition on Mo/HMCM-22 Catalysts for Methane Aromatization: A TP Technique Investigation. *J. Catal.* **2002**, *208*, 260–269. [CrossRef]
26. Weckhuysen, B.M.; Rosynek, M.P.; Lunsford, J.H. Characterization of Surface Carbon Formed during the Conversion of Methane to Benzene over Mo/H-ZSM-5 Catalysts. *Catal. Lett.* **1998**, *52*, 31–36. [CrossRef]
27. Tan, P. Active Phase, Catalytic Activity, and Induction Period of Fe/Zeolite Material in Nonoxidative Aromatization of Methane. *J. Catal.* **2016**, *338*, 21–29. [CrossRef]
28. Ohnishi, R.; Liu, S.; Dong, Q.; Wang, L.; Ichikawa, M. Catalytic Dehydrocondensation of Methane with CO and CO_2 toward Benzene and Naphthalene on Mo/HZSM-5 and Fe/Co-Modified Mo/HZSM-5. *J. Catal.* **1999**, *182*, 92–103. [CrossRef]
29. Hoff, T.C.; Thilakaratne, R.; Gardner, D.W.; Brown, R.C.; Tessonnier, J.P. Thermal Stability of Aluminum-Rich ZSM-5 Zeolites and Consequences on Aromatization Reactions. *J. Phys. Chem. C* **2016**, *120*, 20103–20113. [CrossRef]
30. Deng, Y.; Veser, G. Toward Accelerated Activation of Fe-ZSM-5 in Methane Dehydroaromatization. *Energy Fuels* **2023**, *37*, 13282–13295. [CrossRef]
31. Fals, J.; Toloza, C.A.T.; Puello-Polo, E.; Márquez, E.; Méndez, F.J. A Comprehensive Study of Product Distributions and Coke Deposition during Catalytic Cracking of Vacuum Gas Oil over Hierarchical Zeolites. *Heliyon* **2023**, *9*, e15408. [CrossRef]
32. Mirabella, F.M. *Modern Techniques in Applied Molecular Spectroscopy*; Wiley: Hoboken, NJ, USA, 1998; ISBN 0471123595.

33. Jia, L.Y.; Farouha, A.; Pinard, L.; Hedan, S.; Comparot, J.D.; Dufour, A.; Ben Tayeb, K.; Vezin, H.; Batiot-Dupeyrat, C. New Routes for Complete Regeneration of Coked Zeolite. *Appl. Catal. B* **2017**, *219*, 82–91. [CrossRef]
34. Julian, I.; Ramirez, H.; Hueso, J.L.; Mallada, R.; Santamaria, J. Non-Oxidative Methane Conversion in Microwave-Assisted Structured Reactors. *Chem. Eng. J.* **2019**, *377*, 119764. [CrossRef]
35. Ano, T.; Tsubaki, S.; Liu, A.; Matsuhisa, M.; Fujii, S.; Motokura, K.; Chun, W.J.; Wada, Y. Probing the Temperature of Supported Platinum Nanoparticles under Microwave Irradiation by in Situ and Operando XAFS. *Commun. Chem.* **2020**, *3*, 86. [CrossRef] [PubMed]